PAPER

Check for updates

Aqueous-phase detection of antibiotics and nitroaromatic explosives by an alkali-resistant Zn-MOF directed by an ionic liquid†

Jian-Hua Qin, [ID] [a] Ya-Dan Huang, [ab] Ming-Yu Shi, [a] Hua-Rui Wang, *[a] Min-Le Han, [a] Xiao-Gang Yang, [ID] *[a] Fei-Fei Li [b] and Lu-Fang Ma [ID] [ac]

An alkali-resistant Zn-MOF directed by [BMI]Br ionic liquid, $(BMI)_2[Zn_3(ptptc)_2]$ (1), based on a π-electron-rich terphenyl-tetracarboxylic acid, has been synthesized under the combination of hydro/solvothermal and ionothermal condition (BMI = 1-butyl-3-methylimidazolium, H_4ptptc = *p*-terphenyl-3,3″,5,5″-tetracarboxylic acid). In **1**, the trinuclear Zn(II) clusters are linked by the organic moieties of the ptptc ligands, resulting in a 3D anionic framework structure with highly disordered $[BMI]^+$ cations filled in the pores. **1** exhibits good chemical stability in water and NaOH solutions (pH range of 7–12), which allow it to detect antibiotics and nitroaromatic explosives in an aquatic system. **1** represents high fluorescence quenching efficiency toward NFs (furazolidone, FZD; nitrofurazone, NZF; nitrofurantoin, NFT), NMs (ronidazole, RDZ; metronidazole, MDZ; dimetridazole, DTZ; ornidazole, ODZ) and nitrophenol (2-nitrophenol, 2-NP; 3-nitrophenol, 3-NP; 4-nitrophenol, 4-NP; 2,4,6-trinitrophenol, TNP) in water solution, respectively.

Introduction

Antibiotics and nitroaromatic explosives, widely used in the clinic and in industry, have been noticed as undesirable organic pollutants in wastewater as well as drinking water, threatening the security of the environment and society.[1,2] The abuse of antibiotics, particularly nitro-based antibiotics such as nitrofurans (NFs) and nitroimidazole (NMs), releases antibiotic residues in the environment, which are harmful to the health of humans and wildlife, due to their degradation products and toxicity.[1] On the other hand, nitroaromatic explosives such as nitrophenols and 2-nitrotoluene (2-NT), 2,4-dinitrotoluene (2,4-DNT), are primary ingredients of industrial explosives and environmentally deleterious substances.[2–4] Among all nitroaromatics, nitrophenols pose significant health risks on account of their physiologically active and potentially carcinogenic.[3,4] 2-nitrophenol (2-NP) and 4-nitrophenol (4-NP) have been listed as "Priority Pollutants" on the US Environmental Protection Agency's (USEPA's) list.[4] Therefore, the efficient detection of antibiotics and explosives in water is a pressing challenge targeted at appropriate environmental monitoring.

Since the first work reported in 2009 by Li,[5] luminescent metal–organic frameworks (LMOFs), based on the electron transfer and/or energy transfer mechanisms, have been demonstrated as promising alternatives to detect trace amounts of various nitroaromatics explosives.[6–11] Also, Zhou and Li have recently reported two new chemically stable fluorescent Zr(IV)-based MOFs as sensing materials to detect antibiotics for the first time.[12] LMOF sensor materials have advantages in terms of distinct luminescence spectrum, portability, short response times, high selectivity and sensitivity, applicability in both the solid and solution phase.[5–15] However, due to the poor stability of LMOFs in water or in acidic/basic medium, most of them were checked in organic solvents instead of water.[5–14] The kind of metal, organic ligand, guest as well as the topology of structure all play key roles in the physical or chemical properties of MOFs, such as water stability, ionic character, hydrophobicity, polarizability, pore apertures *etc*, which are crucial for achieving the targeted sensing application.[10,11,16,17] Generally, implantation of π-conjugated organic group into the shaped ligand further extended to the framework, resulting in the smaller HOMO–LUMO energy gap, is an efficient way to enhance targeted property of MOFs and beneficial for sensing performance.[10,11]

[a]College of Chemistry and Chemical Engineering, Henan Key Laboratory of Function-Oriented Porous Materials, Luoyang Normal University, Luoyang 471934, China. E-mail: wanghrly@126.com; yxg2233@126.com

[b]College of Chemistry and Chemical Engineering, Henan Polytechnic University, Jiaozuo, 454000, PR. China

[c]College of Chemistry and Molecular Engineering, Zhengzhou University, Zhengzhou, 450001, PR. China

† Electronic supplementary information (ESI) available: Sturcture figure, TG plot, fluorescence spectra, phosphorescence spectra, details of detecting of the selected antibiotics and nitroaromatic explosives, crystal data, selected bond lengths and angles, summary of quenching constants, HOMO and LUMO energies calculated for the analytes. CCDC 1959055. For ESI and crystallographic data in CIF or other electronic format see DOI: 10.1039/c9ra08733h

Ionic liquids (ILs), as a type of ionic compounds, have received increasing attention as green solvent for the syntheses of MOFs due to their peculiar physical properties.[18–23] In comparison with the traditional hydro/solvothermal procedure by using only water and/or organic solvents, the specific ionic environment of ILs would lead to the formation of novel MOFs that can not (or not easily) be obtained in molecular solvents. Relevant researches showed that the cation and the anion species can individually or cooperatively influence the resulting structures, due to the highly structured liquid with relatively long-range correlations. ILs could serve as a template directing agent even though neither the cation nor anion being occluded into the ultimate structure, facilitate the formation of condensed structure, obviously improve crystal quality and yield, and stimulate the structure conversion from a hetero-chiral coaxially nested double-helical column to a cationic spiral staircase.[23] Our group have reported three types of lanthanide MOFs, all of which show excellent water-stability that probably can be attributed to the condensed structure directed by ILs, protecting these MOFs from the ingress of water.[23b,23c,23e]

We are particularly interested in using ILs to mediate novel MOFs with hydrolytic stability for water related applications.[23b,23c,23e] Herein, we report an alkali-resistant 3D porous Zn-MOF directed by [BMI]Br IL, $(BMI)_2[Zn_3(ptptc)_2]$ (1) (BMI = 1-butyl-3-methylimidazolium, H_4ptptc = p-terphenyl-$3,3'',5,5''$-tetracarboxylic acid), for aqueous-phase detection of antibiotics and nitroaromatic explosives. H_4ptptc has been extensively employed for the constructions of MOFs.[24–26] As shown in Scheme 1, three types of Zn-MOFs based on H_4ptptc ligand have been fabricated in molecular solvents, with different topologies involving diamond (**dia**), lonsdaleite (**lon**) and **nbo**.[24] These three 4-connected topology frameworks based binuclear Zn clusters show poor stability in water.[24] However, trinuclear Zn(II) clusters were formed in 1, leading to the condensed (4,8)-connected CaF_2 topology with excellent hydrolytic stability. 1 exhibits high thermal stability and good chemical stability in water and NaOH solutions (pH range of 7–12), which allow it to detect antibiotics and nitroaromatic explosives in an aquatic system. It has been found that 1 represents high fluorescence quenching efficiency toward NFs (furazolidone, FZD; nitro-furazone, NZF; nitrofurantoin, NFT), NMs (ronidazole, RDZ; metronidazole, MDZ; dimetridazole, DTZ; ornidazole, ODZ) and nitrophenol (2-nitrophenol, 2-NP; 3-nitrophenol, 3-NP; 4-nitro-phenol, 4-NP; 2,4,6-trinitrophenol, TNP) in water solution, respectively.

Experimental section

Materials and physical measurements

All reagents were of analytical grade and obtained from commercial sources without further purification. Elemental analysis for C and H were performed on a PerkinElmer 240 elemental analyzer. Thermal analyses were performed on a SDT 2960 thermal analyzer from room temperature to 800 °C at a heating rate of 20 °C min^{-1} under nitrogen flow. Powder X-ray diffraction (PXRD) data were collected on a Rigaku D/Max-

2500PC diffractometer with Cu Kα radiation ($\lambda = 1.5406$ Å) over the 2θ range of 5–50° with a scan speed of 5° min^{-1} at room temperature. Room temperature PL spectra and time-resolved lifetime were conducted on an Edinburgh FLS1000 fluorescence spectrometer equipped with a xenon arc lamp (Xe900), nanosecond flash-lamp (nF900) and a microsecond flashlamp with time-resolved single photon counting-multi-channel scaling (MCS) mode. Fluorescence spectra for the aqueous solutions of each analyte were recorded on a Hitachi 850 fluorescence spectrophotometer.

Synthesis of $(BMI)_2[Zn_3(ptptc)_2]$ (1)

First step. $ZnCl_2$ (0.2 mmol) and H_4ptptc (0.10 mmol) were soaked in 1 mL [BMI]Br solutions in a glass vial (10 mL), and heated in an isotherm oven more than 100 °C until starting materials dissolved.

Second step. 4 mL mixed solvent of acetonitrile (CH_3CN) and H_2O (V/V = 1 : 1) was added, and then the homogeneous phase was transferred to a 25 mL Teflon-lined stainless steel vessel. The vessel was sealed and heated to 160 °C for 72 h and then cooled to room temperature at a rate of 5 °C h^{-1}. Colorless block crystals of 1 were obtained in high yields (∼90%). Elemental analysis calcd (%) for 1 $C_{60}H_{50}N_4O_{16}Zn_3$ (1279.21): C 56.34, H 3.94, N 4.38. Found: C 55.87, H 3.76, N 4.18.

X-ray crystallography

Single crystal X-ray diffraction analysis of 1 was carried out on an Oxford Diffraction Super Nova area-detector diffractometer using mirror optics monochromated Mo Kα radiation ($\lambda = 0.71073$ Å) at room temperature. Using Olex2,[27] the structure was solved with the ShelXT[28] structure solution program using Intrinsic Phasing and refined with the ShelXL[29] refinement package using least squares minimisation. The hydrogen atoms were assigned with common isotropic displacement factors and included in the final refinement by use of geometrical restrains. The [BMI]$^+$ cations were disordered and could not be located. The diffuse electron densities in the structure were therefore treated using the SQUEEZE routine in the program PLATON. The crystallographic data and selected bond lengths and angles for 1 are listed in Tables S1 and S2 in ESI.† Crystallographic data for the structural analyses have been deposited with the Cambridge Crystallographic Data Center. CCDC numbers for 1 is 1959055.

Experiments of detecting of antibiotics and nitroaromatic explosives in the aqueous phase

The fluorescence property of 1 was investigated in water emulsions at room temperature. The fine grinding MOF powder (2 mg) was dispersed in saturated aqueous solutions or a certain concentration (2 mL) of a series of antibiotics (0.1 mM) and nitroaromatics (1 mM), treated by ultrasonication for 30 min and then aged for 3 days to form a stable emulsion before the fluorescence studies. Twelve kinds of antibiotics, nitrofurazone (NZF), dimetridazole (DTZ), ornidazole (ODZ), nitrofurantoin (NFT), ronidazole (RDZ), chloramphenicol (CAP), sulfamethazine (SMZ), metronidazole (MDZ), furazolidone (FZD),

sulfadiazine (SDZ), penicillin (PCL), and florfenicol (FFC), were detected. The nitroaromatics used in this study were 2-nitrophenol (2-NP), 3-nitrophenol (3-NP), 4-nitrophenol (4-NP), 2,4,6-trinitrophenol (TNP), nitrobenzene (NB), 2-nitrotoluene (2-NT), 2,4-dinitrotoluene (2,4-DNT), and 1,3-dintrobenzene (1,3-DNB). In fluorescence titration setup, 2 mg of 1 was dispersed in 2 mL aqueous solution, treated by ultrasonication for 30 min and then aged for 3 days for the next experiment. The fluorescence was measured *in situ* after incremental addition of freshly prepared 1 mM or saturated aqueous solutions of each analyte. The mixed solution was stirred at a constant rate during experiment to maintain its homogeneity. All the experiments were performed in triplicate and consistent results are reported. The quenching efficiency (%) was estimated using the formula $(F_0 - F)/F_0 \times 100\%$, where F_0 and F are the maximum fluorescent intensity of 1 before and after the addition of analyte, respectively.

Results and discussion

Synthesis and crystal structure

The reaction of H_4ptptc with $ZnCl_2$ in a mixture of acetonitrile (CH_3CN)/H_2O/[BMI]Br (2/2/1) at 160 °C yields a novel type of Zn-MOF. The mineralizing agent [BMI]Br aids the solubility of the starting materials, and is required for high yields. Systematic exploration of several molecular solvents shows that 1 is only formed in CH_3CN–H_2O mixture. Other solvents, such as DMF or H_2O or CH_3CN, or DMF–H_2O mixed solvent were also attempted, but only fine powder products were obtained. Besides, when using $Zn(NO_3)_2$ or $ZnSO_4$ or other zinc(II) salts, only much unspecified impurities were obtained. In a typical synthesis procedure, we firstly dissolve $ZnCl_2$ and H_4ptptc in [BMI]Br, followed by adding CH_3CN–H_2O into the reaction system, and perform the reaction at 160 °C for 3 days. This facile procedure can produce crystals of 1 with a high yield and high crystal quality.

Single crystal X-ray analysis indicates that 1 crystallizes in triclinic crystal system P$\bar{1}$ space group. The asymmetry unit of 1 is composed of three crystallographically independent Zn(II) ions, two ptptc ligands and two free [BMI]$^+$ cations. As shown in Fig. 1a, Zn1 coordinates to six oxygen atoms from six carboxylate groups of six different ptptc ligands to complete a distorted octahedral coordination geometry. Zn2 and Zn3 both connect with four oxygen atoms from four carboxylate groups of four different ptptc ligands, resulting in a distorted tetrahedral coordination sphere. Two types ptptc ligands both act as μ_7-bridging, linking seven Zn(II) ions through two μ_2-η^1:η^1, one μ_2-η^0:η^2, and one μ_1-η^0:η^1 coordination modes for four carboxylate groups, respectively. Zn1, Zn2 and Zn3 ions are joined together by eight carboxylate groups of eight ptptc ligands to form a trinuclear [$Zn_3(CO_2)_8$] cluster, in which the Zn⋯Zn separations through carboxylate groups are 3.293 and 3.279 Å for Zn1⋯ Zn2 ($-x$, 1 − y, −z), Zn1⋯Zn3 (1 + x, 1 + y, z), respectively. These trinuclear [$Zn_3(CO_2)_8$] clusters are extended by terphenyl groups of ptptc ligands generating a 3D anionic framework (Fig. 1b). The structure of complex 1 has channels of 7.0 × 8.1 Å dimensions with a void space running along [010] direction, which are occupied by highly disordered [BMI]$^+$ cations as counter charges. Furthermore, topological analysis is carried out to get insight of the structure of 1. If [$Zn_3(CO_2)_8$] cluster is considered as a eight-connected node, and ptptc ligand is regarded as a four-connected node, as shown in Fig. S1 in ESI,† the structure can be viewed as a metal–organic replica of fluorite with (4,8)-connected topology (CaF$_2$).[30]

The role of ILs

Unique physical and solvent properties of ILs may create special crystallization environments and provide structure-directing

Scheme 1 The synthetic routes for Zn-MOFs based on H4ptptc.

Fig. 1 (a) Representation of the Zn(II) coordination environments in **1**. Symmetry codes (A) 1 + X, +Y, +Z; (B) 1 + X, 1 + Y, +Z; (C) −1 + X, +Y, +Z; (D) −1 + X, −1 + Y, +Z; (E) −X, 1 − Y, −Z; (F) 1 − X, 1 − Y, −Z; (G) 1 − X, 2 − Y, −Z; (H) +X, −1 + Y, +Z; (I) 1 − X, 2 − Y, 1 − Z. (b) View of 3D coordination framework of **1**.

agents, which lead to quite different networks from those obtained by traditional hydro/solvothermal methods. Our past studies proved that ILs seem to be promising for the syntheses of novel MOFs that are inaccessible using traditional synthetic routes.[23] As discussed above, [BMI]Br not only serves as solvent and structure-directing agent, but also enters the resulting structure as charge compensating agent.

H$_4$ptptc possesses delocalized π-electron system which not only endows the MOFs with luminescent properties but also encourage π–π stacking to increase the framework stability.[24–26] In addition, four carboxylic acid groups and the rigid terphenyl in H$_4$ptptc can afford varied coordination modes to yield diverse topology structures.[24–26] As shown in Scheme 1, there have been three types of Zn-MOFs based on H$_4$ptptc ligand: [Zn$_2$(ptptc)(DMF)$_3$]·4H$_2$O·5.5DMF (**2**), [Zn$_2$(ptptc)(DMA)(H$_2$O)]·2.5H$_2$O·3.5DMA (**3**) and [Zn(ptptc)$_{0.5}$(H$_2$O)]·DMF·DMA (**4**), which are emanated from the different molecular solvents (DMF, DMA and mixture of DMF/DMA (1 : 1), respectively).[24] The three types of Zn-MOFs present a permanent porosity with considerable potential void volume (about 39%–68% of the total crystal volume). Besides, the yields of the three Zn-MOFs are only about 30%. However, in our experiments, the crystalline product of Zn(II) ions and ptptc ligands turned out to be a condensed structure (BMI)$_2$[Zn$_3$(ptptc)$_2$] (**1**), with good

qualities and high yields (~90%). The major advantage of [BMI]Br can probably tune the solvent properties to match those required for the synthesis of condensed structure.

Besides, different synthesis methods also lead to different topologies. The structures of the above mentioned three Zn-MOFs (**2**, **3** and **4**) and **1** based on H$_4$ptptc ligand are dependent on the different solvents (molecular solvent or ionic liquid). **2**, **3** and **4** all exhibit 4-connected networks (considering binuclear Zn clusters and ptptc ligand both as the 4-connected nodes) with different topologies involving diamond (**dia**), lonsdaleite (**lon**) and **nbo**. However, trinuclear Zn(II) clusters were formed in **1** under the combination of ionothermal and hydro/solvothermal condition (our work). Each trinuclear Zn(II) cluster connects eight ptptc ligands and each ptptc ligand connects four trinuclear Zn(II) clusters, leading to the (4,8)-connected CaF$_2$ topology. Interestingly, the distortion extents of ptptc ligands are found to be dependent on their topologies. Owing to being compressed, the ptptc ligands are seriously distorted in **1**, with the larger dihedral angles between the intermediate benzene ring and adjacent two benzene rings in the ptptc ligand. In **1**, the dihedral angles among the benzene rings in the two types ptptc ligands are 45.90° and 53.24°, 40.286° and 29.86°, respectively. While the dihedral angles in **2**, **3** and **4** are about 30° or 0°, respectively.

Thermal and pH-stability

Considering practical applications, the stabilities of **1** to heat and pH were investigated. Thermogravimetric (TG) analysis shows that the framework of **1** has high thermal stability and start to decompose around 400 °C (Fig. S3 in ESI†). **1** also exhibits good chemical stability and PXRD results have suggested that **1** could remain stable in the pH range of 7–12 for three days (Fig. 2). The presence of a strong peak around 25° in alkali solutions may be due to variation in the preferred orientation of the powder samples during collection of the experimental PXRD data. However, a sharp impurity peak at about 2θ = 6° could be observed in acidic water with pH values of 2 and 6 (Fig. S2 in ESI†).

Fig. 2 PXRD patterns for simulated and experimental **1** sample soaked in aqueous solutions over the pH range from 7 to 12.

Fluorescent properties

Luminescence spectroscopy as well as time-resolved luminescence lifetime in solid state were investigated. **1** displays an emission band at 403 nm, which is blue-shifted relative to the 417 nm band of H$_4$ptptc ligand (Fig. S4 and S5 in ESI†). The fluorescence decay curve of **1** is fitted as a single exponential function with the lifetime of 7.79 ns for peak of 403 nm (Fig. S5 in ESI†). By the excitation of microsecond flash lamp (100 Hz), **1** displays a broad emission with two main peaks at 668 and 710 nm (Fig. S6 in ESI†). Time-resolved measurements revealed long lifetime of 400.48 and 359.26 μs, which can be assigned to phosphorescence emission (Fig. S6 in ESI†). The long lifetime of phosphorescence emission is due to the strong coordination bonds and dense stacking structure of **1** which provide a rigid matrix reducing the nonradiative loss of triplet excitons.[31] We also examined the fluorescent properties of **1** dispersed in water and common organic solvent. As shown in Fig. S7 in the ESI,† the fluorescent emissions of **1** have slight solvent dependence, and **1** shows stronger emissions in H$_2$O and CH$_3$CN, respectively, and the emission spectra are close to those of solid state sample. The strong emission and stability of **1** in H$_2$O suspension indicate potential to be utilized as antibiotics and nitro-aromatic explosives sensor in the aqueous phase.

Detection of antibiotics and nitroaromatics in the aqueous phase

The high water stability together with good dispersibility and strong emissions of the micrometre-sized fine particles of **1** in water suspension, prompt us to explore its application in monitoring antibiotics and nitroaromatics in water. The fine grinding sample **1** was dispersed in 0.1 mM aqueous solutions

of the selected twelve kinds of antibiotics. **1** has high quenching efficiencies toward NZF and DTZ, but very poor toward PCL and FFC (Fig. 3a, b and S8 in ESI†). Fig. 3b shows the percentage of fluorescence quenching in terms of adding a certain amount of different antibiotics at room temperature. NZF and DTZ give rise to the highest quenching efficiencies of 97 and 90%, respectively. ODZ, NFT, RDZ, CAP, SMZ, and MDZ also lead to relative high quenching efficiencies (>50%), whereas quenching efficiencies are low for the remaining antibiotics. To examine sensing sensitivity towards these antibiotics in more detail, fluorescence-quenching titrations were performed with gradually adding a certain amount of the analytes to suspensions of **1**. For NZF, DTZ ODZ, NFT, RDZ, and FZD, the fluorescence quenching efficiency increased drastically with the analyte amount even in the low concentration range (Fig. 3c, S9–S20 in ESI†). The quenching efficiency can be quantitatively explained by the Stern–Volmer equation: $(F_0/F) = K_{sv}[Q] + 1$, where K_{sv} is the quenching constant (ppm^{-1}), [Q] is the concentration of the analyte, F_0 and F are the fluorescent intensities before and after addition of the analyte, respectively. As indicated in Fig. S9–S20 in ESI,† the SV plots for the above-mentioned six kinds of antibiotics are nearly linear at low concentrations, and subsequently deviate from linearity, bending upwards at higher concentrations. Such phenomena of nonlinear SV plots might be attributed to self-absorption, a combination of static and dynamic quenching, or an energy-transfer process between the analytes and the MOFs.[32] Linear SV plots are observed for all the other antibiotics over a wide concentration range. The higher K_{sv} values are 1.7×10^{-1} ppm^{-1} for NZF and 1.6×10^{-1} ppm^{-1} for DTZ, respectively, as verified by linear fitting of the SV plots at a low concentration range (Table S3 in ESI†). These K_{sv} values
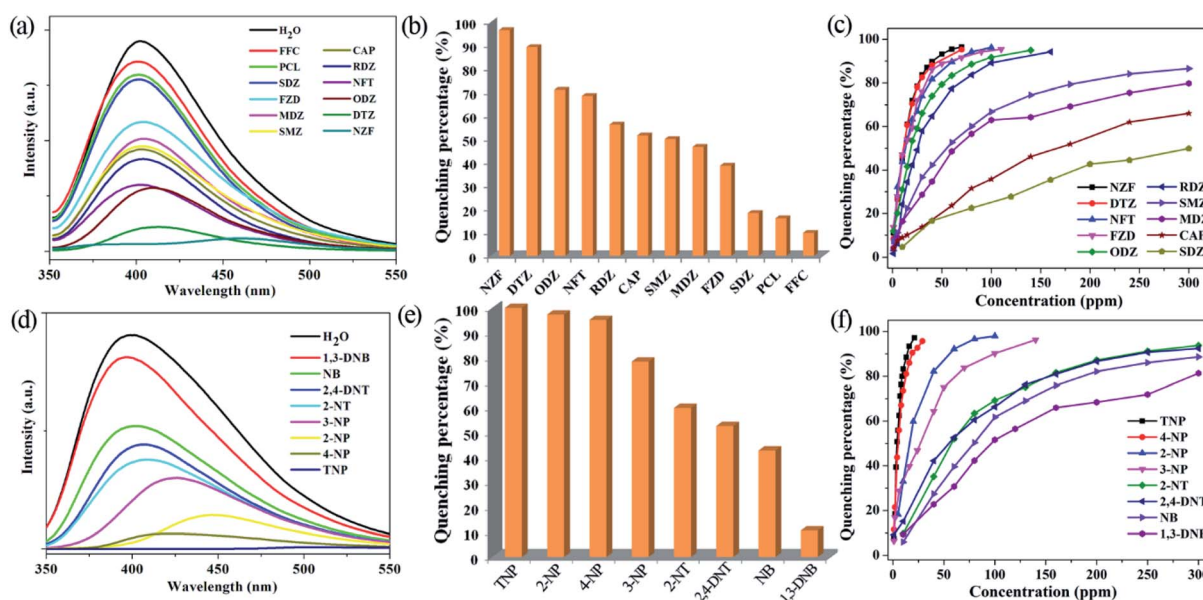

Fig. 3 The emission spectra for **1** dispersed in 0.1 mM aqueous solutions of the selected antibiotics (a) and 1 mM aqueous solutions of the selected nitroaromatics explosives (d). Quenching efficiency of the fluorescent intensity for **1** dispersed in 0.1 mM aqueous solutions of the selected antibiotics (b) and 1 mM aqueous solutions of the selected nitroaromatics explosives (e). Quenching efficiencies of **1** dispersed in aqueous solutions at different concentrations of the selected antibiotics (c) and nitroaromatics explosives (f).

are comparable to those of Zr(IV)-based MOFs reported by Zhou and Li.[12]

To date, a number of MOFs have been employed for various nitroaromatics explosives detection, but most of them work in organic solvent systems, not in water, due to the poor water stabilities of MOFs.[5–14] The fine grinding sample **1** was dispersed in 1 mM or saturated aqueous solutions of a series of nitroaromatics. Significant fluorescence quenching of **1** occurs upon the addition of the selected four nitrophenol compounds (TNP, 2-NP, 4-NP and 3-NP), while 1,3-DNB shows a very low quenching effect (Fig. 3d, e and S21 in ESI†). As depicted in Fig. 3e, more than 95% of quenching efficiency could be achieved for TNP, 2-NP and 4-NP. In addition, 2-NT, 2,4-DNT and NB also lead to relative high quenching efficiencies (about 40–60%). The quenching efficiencies of **1** for the eight nitroaromatics follow the order of TNP > 2-NP > 4-NP > 3-NP > 2-NT > 2,4-DNT > NB > 1,3-DNB. In fluorescence titration, **1** shows fast detection and high fluorescence quenching for the nitrophenol compounds on incremental addition of 20 ppm for TNP, 30 ppm for 4-NP, 90 ppm for 2-NP and 140 ppm for 3-NP, respectively (Fig. 3f and S22–S25 in ESI†). Similar to those in detecting antibiotics, the SV plots for the four nitrophenol compounds are also nearly linear at low concentrations and subsequently deviated from linearity and bend upwards at higher concentrations (Fig. S22–S25 in ESI†). Whereas, the other nitroaromatics give linear SV plots over a wide concentration range (Fig. S26–S29, in the ESI†). **1** shows the higher K_{sv} values of 5.3×10^{-1} ppm^{-1} for TNP and 3.8×10^{-1} ppm^{-1} for 4-NP, respectively (Table S3 in ESI†). In addition, the K_{sv} value for TNP in **1** is significantly larger than that of our reported lanthanide MOFs, demonstrating a super quenching ability of **1**.[23b,23c,23e]

The fluorescence quenching mechanism of nitro compounds

Generally, photoinduced electron transfer and/or energy transfer are regarded as the fluorescence quenching mechanism.[5–14] Molecular orbital calculation can also be used to describe the valence-band (VB) and conduction-band (CB) energy levels of MOFs.[5,6] In most cases, the CB energy levels of MOFs are higher than the lowest unoccupied molecular orbitals (LUMOs) of nitro compounds, which are low-lying π*-type orbitals stabilized by the NO$_2$ group through conjugation. This facilitates electron transfer from the electron-rich framework to the LUMO of the electron-deficient nitro compounds upon photoexcitation, leading to fluorescence quenching.[5–14] Fig. 4 shows the HOMO and LUMO orbital energies of antibiotics and nitroaromatics.[8a,12,13b] The lower the LUMO energy of the nitro compounds, the more easily electron transfer occurs and the higher quenching efficiency can be observed. In fluorescence titration processes, the maximum quenching efficiency observed for the four nitrophenol compounds (TNP, 2-NP, 4-NP and 3-NP), NZF and NFT are in good agreement with the LUMO energy levels of nitro analytes, but the order of observed quenching efficiency is not fully in accordance with the LUMO energies of other antibiotics and nitroaromatics. Thus, the photoinduced electron transfer is not the only mechanism, and an energy transfer should also exist in the fluorescence quenching processes observed in these systems.

The nonlinearity of the SV plots for the four nitrophenol compounds, NZF and NFT, i.e., further indicate the existence of the resonance energy transfer from the MOF to these nitro compounds. A necessary condition of such energy transfer is the effective overlap between the absorption band of the analyte and the emission band of the MOF.[5–14] The UV-vis absorption spectra of antibiotics and nitroaromatics in aqueous solution were measured. As shown in Fig. S30 in ESI,† the greatest spectral overlap between the absorption spectrum of NZF, NFT and FZD and the emission spectrum of **1** can be observed. For nitroaromatics, TNP has the greatest overlap, followed by 4-NP, 3-NP and 2-NP, while negligible spectral overlap for other nitroaromatics 1,3-DNB, NB, 2,4-DNT and 2-NT (Fig. S31 in ESI†). These results indicate that the long-range energy transfer may also play a key role in the fluorescence quenching process.[5–14] As a result, **1** exhibits higher fluorescence quenching response towards the four nitrophenol compounds, NZF, NFT and FZD, owing to the coexistence of electron transfer and energy transfer.

(a)

(b)

Fig. 4 HOMO and LUMO energy levels for the selected antibiotics (a) and nitroaromatics explosives (b).

Paper

Conclusions

In summary, an alkali-resistant Zn-MOF based on a π-electron-rich terphenyl-tetracarboxylic acid, (BMI)$_2$[Zn$_3$(ptptc)$_2$] (**1**), has been synthesized under the combination of hydro/solvothermal and ionothermal condition. [BMI]Br not only serves as solvent to dissolve both organic and inorganic precursors and improve crystal yield compared to other ptptc-based Zn-MOFs, but also acts as structure-directing agent to mediate novel MOF. **1** exhibits good chemical stability in water and alkaline solution, which allow it to be used in an aquatic system. **1** shows remarkable sensitivity for nitro-explosives in a wide scope, particularly for phenol hydroxyl-containing nitro-explosives. Besides, **1** also displays a highly quenching response to antibiotics at fairly low responsive concentration. The orbital energy theoretical calculation and UV-vis absorption experiments indicate that quenching mechanism might be attributed to photo-induced electron transfer and fluorescence resonance energy transfer from the excited MOF to the electron deficient analytes adsorbed on the particles surface of **1**.

Conflicts of interest

There are no conflicts to declare.

Acknowledgements

Notes and references

1 (a) Q.-Q. Zhang, G.-G. Ying, C.-G. Pan, Y.-S. Liu and J.-L. Zhao, *Environ. Sci. Technol.*, 2015, **49**, 6772–6782; (b) H. Wang, N. Wang, J. Qian, L. Hu, P. Huang, M. Su, X. Yu, C. Fu, F. Jiang, Q. Zhao, Y. Zhou, H. Lin, G. He, Y. Chen and Q. Jiang, *Environ. Sci. Technol.*, 2017, **51**, 3518–3525.

2 (a) M. E. Germain and M. J. Knapp, *Chem. Soc. Rev.*, 2009, **38**, 2543–2555; (b) Y. Salinas, R. Martínez-Máñez, M. D. Marcos, F. Sancenón, A. M. Costero, M. Parra and S. Gil, *Chem. Soc. Rev.*, 2012, **41**, 1261–1296.

3 (a) K. Karim and S. K. Gupta, *Water Res.*, 2003, **37**, 2953–2959; (b) Z. She, M. Gao, C. Jin, Y. Chen and J. Yu, *Process Biochem.*, 2005, **40**, 3017–3024.

4 V. Uberoi and S. K. Bhattacharya, *Water Environ. Res.*, 1997, **69**, 146–156.

5 A. Lan, K. Li, H. Wu, D. H. Olson, T. J. Emge, W. Ki, M. Hong and J. Li, *Angew. Chem., Int. Ed.*, 2009, **48**, 2334–2338.

6 (a) S. Pramanik, C. Zheng, X. Zhang, T. J. Emge and J. Li, *J. Am. Chem. Soc.*, 2011, **133**, 4153–4155; (b) Z. Hu, K. Tan, W. P. Lustig, H. Wang, Y. Zhao, C. Zheng, D. Banerjee, T. J. Emge, Y. J. Chabal and J. Li, *Chem. Sci.*, 2014, **5**, 4873–4877.

7 (a) D. Tian, Y. Li, R.-Y. Chen, Z. Chang, G.-Y. Wang and X.-H. Bu, *J. Mater. Chem. A*, 2014, **2**, 1465–1470; (b) X. J. Liu, X. Wang, J. L. Xu, D. A. Tian, R. Y. Chen, J. Xu and X. H. Bu, *Dalton Trans.*, 2017, **46**, 4893–4897.

8 (a) S. S. Nagarkar, B. Joarder, A. K. Chaudhari, S. Mukherjee and S. K. Ghosh, *Angew. Chem., Int. Ed.*, 2013, **52**, 2881–2885; (b) A. Karmakar, A. Kumar, A. K. Chaudhari, P. Samanta, A. V. Desai, R. Krishna and S. K. Ghosh, *Chem.–Eur. J.*, 2016, **22**, 4931–4937.

9 (a) L. H. Cao, F. Shi, W. M. Zhang, S. Q. Zang and T. C. W. Mak, *Chem.–Eur. J.*, 2015, **21**, 15705–15712; (b) G. X. Wen, M. L. Han, X. Q. Wu, Y. P. Wu, W. W. Dong, J. Zhao, D. S. Li and L. F. Ma, *Dalton Trans.*, 2016, **45**, 15492–15499; (c) H. R. Fu, X. X. Wu, L. F. Ma, F. Wang and J. Zhang, *ACS Appl. Mater. Interfaces*, 2018, **10**, 18012–18020; (d) L.-H. Xie, X.-M. Liu, T. He and J.-R. Li, *Chem*, 2018, **4**, 1911–1927; (e) H. He, Q.-Q. Zhu, F. Sun and G. Zhu, *Cryst. Growth Des.*, 2018, **18**, 5573–5581.

10 (a) Y. Cui, Y. Yue, G. Qian and B. Chen, *Chem. Rev.*, 2012, **112**, 1126–1162; (b) L. E. Kreno, K. Leong, O. K. Farha, M. Allendorf, R. P. Van Duyne and J. T. Hupp, *Chem. Rev.*, 2012, **112**, 1105–1125; (c) D. Banerjee, Z. Hu and J. Li, *Dalton Trans.*, 2014, **43**, 10668–10685; (d) Y. Cui, B. Chen and G. Qian, *Coord. Chem. Rev.*, 2014, **273–274**, 76–86; (e) Z. Hu, B. J. Deibert and J. Li, *Chem. Soc. Rev.*, 2014, **43**, 5815–5840.

11 (a) W. P. Lustig, S. Mukherjee, N. D. Rudd, A. V. Desai, J. Li and S. K. Ghosh, *Chem. Soc. Rev.*, 2017, **46**, 3242–3285; (b) Y. Zhang, S. Yuan, G. Day, X. Wang, X. Yang and H.-C. Zhou, *Coord. Chem. Rev.*, 2018, **354**, 28–45; (c) J. He, J. Xu, J. Yin, N. Li and X.-H. Bu, *Sci. China Mater.*, 2019, **62**, 1655–1678; (d) P. L. Wang, L. H. Xie, E. A. Joseph, J. R. Li, X. O. Su and H. C. Zhou, *Chem. Rev.*, 2019, **119**, 10638–10690.

12 B. Wang, X. L. Lv, D. W. Feng, L. H. Xie, J. Zhang, M. Li, Y. B. Xie, J. R. Li and H. C. Zhou, *J. Am. Chem. Soc.*, 2016, **138**, 6204–6216.

13 (a) M.-L. Han, G.-X. Wen, W.-W. Dong, Z.-H. Zhou, Y.-P. Wu, J. Zhao, D.-S. Li, L.-F. Ma and X. Bu, *J. Mater. Chem. C*, 2017, **5**, 8469–8474; (b) H. R. Fu, L. B. Yan, N. T. Wu, L. F. Ma and S. Q. Zang, *J. Mater. Chem. A*, 2018, **6**, 9183–9191; (c) H. R. Fu, Y. Zhao, T. Xie, M. L. Han, L. F. Ma and S. Q. Zang, *J. Mater. Chem. C*, 2018, **6**, 6440–6448; (d) X. Liu, B. Liu, G. Li and Y. Liu, *J. Mater. Chem. A*, 2018, **6**, 17177–17185; (e) Z.-H. Zhou, W.-W. Dong, Y.-P. Wu, J. Zhao, D.-S. Li, T. Wu and X.-h. Bu, *Inorg. Chem.*, 2018, **57**, 3833–3839.

14 (a) Z.-S. Qin, W.-W. Dong, J. Zhao, Y.-P. Wu, Q. Zhang and D.-S. Li, *Inorg. Chem. Front.*, 2018, **5**, 120–126; (b) Y. Zhou, Q. Yang, D. Zhang, N. Gan, Q. Li and J. Cuan, *Sens. Actuators, B*, 2018, **262**, 137–143; (c) Z. Zhou, M.-L. Han, H.-R. Fu, L.-F. Ma, F. Luo and D.-S. Li, *Dalton Trans.*, 2018, **47**, 5359–5365; (d) J.-H. Wei, J.-W. Yi, M.-L. Han, B. Li, S. Liu, Y.-P. Wu, L.-F. Ma and D.-S. Li, *Chem.–Asian J.*, 2019, **14**, 3694–3701.

15 (a) R.-W. Huang, Y.-S. Wei, X.-Y. Dong, X.-H. Wu, C.-X. Du, S.-Q. Zang and T. C. W. Mak, *Nat. Chem.*, 2017, **9**, 689–697; (b) Y.-P. Wu, G.-W. Xu, W.-W. Dong, J. Zhao, D.-S. Li, J. Zhang and X. Bu, *Inorg. Chem.*, 2017, **56**, 1402–1411; (c) M. M. Xu, X. J. Kong, T. He, X. Q. Wu, L. H. Xie and J. R. Li, *Inorg. Chem.*, 2018, **57**, 14260–14268; (d) K. Fan, S.-S. Bao, W.-X. Nie, C.-H. Liao and L.-M. Zheng, *Inorg.*

Chem., 2018, **57**, 1079–1089; (*e*) B. J. C. Wong, D.-m. Xu, S.-S. Bao, L.-M. Zheng and J. Lei, *ACS Appl. Mater. Interfaces*, 2019, **11**, 12986–12992.

16 (*a*) H. L. Jiang, D. Feng, K. Wang, Z. Y. Gu, Z. Wei, Y. P. Chen and H. C. Zhou, *J. Am. Chem. Soc.*, 2013, **135**, 13934–13938; (*b*) S. M. T. Abtab, D. Alezi, P. M. Bhatt, A. Shkurenko, Y. Belmabkhout, H. Aggarwal, L. J. Weselinski, N. Alsadun, U. Samin, M. N. Hedhili and M. Eddaoudi, *Chem*, 2018, **4**, 94–105; (*c*) E. A. Kapustin, *Chem*, 2018, **4**, 16–17; (*d*) L. N. McHugh, M. J. McPherson, L. J. McCormick, S. A. Morris, P. S. Wheatley, S. J. Teat, D. McKay, D. M. Dawson, C. E. F. Sansome, S. E. Ashbrook, C. A. Stone, M. W. Smith and R. E. Morris, *Nat. Chem.*, 2018, **10**, 1096–1102; (*e*) J.-W. Ye, X.-Y. Li, H.-L. Zhou and J.-P. Zhang, *Sci. China: Chem.*, 2018, **62**, 341–346.

17 (*a*) J. Cui, Y. Li, Z. Guo and H. Zheng, *Chem. Commun.*, 2013, **49**, 555–557; (*b*) H.-R. Fu, F. Wang and J. Zhang, *Dalton Trans.*, 2015, **44**, 2893–2896; (*c*) Y.-N. Gong, T. Ouyang, C.-T. He and T.-B. Lu, *Chem. Sci.*, 2016, **7**, 1070–1075; (*d*) Y. L. Hu, M. L. Ding, X. Q. Liu, L. B. Sun and H. L. Jiang, *Chem. Commun.*, 2016, **52**, 5734–5737.

18 (*a*) E. Ahmed and M. Ruck, *Dalton Trans.*, 2011, **40**, 9347–9357; (*b*) D. Freudenmann, S. Wolf, M. Wolff and C. Feldmann, *Angew. Chem., Int. Ed.*, 2011, **50**, 11050–11060; (*c*) J. Zhang, L. Peng and B. Han, *Soft Matter*, 2014, **10**, 5861–5868; (*d*) B. Zhang, J. Zhang and B. Han, *Chem.–Asian J.*, 2016, **11**, 2610–2619.

19 (*a*) K. Jin, X. Huang, L. Pang, J. Li, A. Appel and S. Wherland, *Chem. Commun.*, 2002, 2872–2873; (*b*) D. N. Dybtsev, H. Chun and K. Kim, *Chem. Commun.*, 2004, 1594–1595; (*c*) J. Zhang, S. Chen and X. Bu, *Angew. Chem., Int. Ed.*, 2008, **47**, 5434–5437; (*d*) S. M. Chen, J. Zhang, T. Wu, P. Y. Feng and X. H. Bu, *J. Am. Chem. Soc.*, 2009, **131**, 16027–16029; (*e*) J. Zhang, T. Wu, S. Chen, P. Feng and X. Bu, *Angew. Chem., Int. Ed.*, 2009, **48**, 3486–3490.

20 (*a*) H. Ren, T. Ben, E. Wang, X. Jing, M. Xue, B. Liu, Y. Cui, S. Qiu and G. Zhu, *Chem. Commun.*, 2010, **46**, 291–293; (*b*) W. X. Chen, H. R. Xu, G. L. Zhuang, L. S. Long, R. B. Huang and L. S. Zheng, *Chem. Commun.*, 2011, **47**, 11933–11935; (*c*) Y. Kang, S. Chen, F. Wang, J. Zhang and X. Bu, *Chem. Commun.*, 2011, **47**, 4950–4952; (*d*) Q.-Y. Liu, Y.-L. Wang, N. Zhang, Y.-L. Jiang, J.-J. Wei and F. Luo, *Cryst. Growth Des.*, 2011, **11**, 3717–3720; (*e*) D.-Y. Du, J.-S. Qin, C.-X. Sun, X.-L. Wang, S.-R. Zhang, P. Shen, S.-L. Li, Z.-M. Su and Y.-Q. Lan, *J. Mater. Chem.*, 2012, **22**, 19673; (*f*) J. Liu, F. Zhang, X. Zou, G. Yu, N. Zhao, S. Fan and G. Zhu, *Chem. Commun.*, 2013, **49**, 7430–7432.

21 (*a*) J. Liu, X. Zou, C. Liu, K. Cai, N. Zhao, W. Zheng and G. Zhu, *CrystEngComm*, 2016, **18**, 525–528; (*b*) Y. Li, Z. Yang, Y. Wang, Z. Bai, T. Zheng, X. Dai, S. Liu, D. Gui, W. Liu, M. Chen, L. Chen, J. Diwu, L. Zhu, R. Zhou, Z. Chai, T. E. Albrecht-Schmitt and S. Wang, *Nat. Commun.*, 2017, **8**, 1354; (*c*) X. X. Sang, J. L. Zhang, J. F. Xiang, J. Cui, L. R. Zheng, J. Zhang, Z. H. Wu, Z. H. Li, G. Mo, Y. Xu, J. L. Song, C. C. Liu, X. N. Tan, T. Luo, B. X. Zhang and B. X. Han, *Nat. Commun.*, 2017, **8**, 7; (*d*) T. Zheng, Z. Yang, D. Gui, Z. Liu, X. Wang, X. Dai, S. Liu,

L. Zhang, Y. Gao, L. Chen, D. Sheng, Y. Wang, J. Diwu, J. Wang, R. Zhou, Z. Chai, T. E. Albrecht-Schmitt and S. Wang, *Nat. Commun.*, 2017, **8**, 15369.

22 (*a*) W.-W. Xiong, J.-R. Li, B. Hu, B. Tan, R.-F. Li and X.-Y. Huang, *Chem. Sci.*, 2012, **3**, 1200; (*b*) Z. P. Wang, J. Y. Wang, J. R. Li, M. L. Feng, G. D. Zou and X. Y. Huang, *Chem. Commun.*, 2015, **51**, 3094–3097.

23 (*a*) J. H. Qin, Y. Jia, H. Li, B. Zhao, D. Wu, S. Zang, H. Hou and Y. Fan, *Inorg. Chem.*, 2014, **53**, 685–687; (*b*) J. H. Qin, B. Ma, X.-F. Liu, H.-L. Lu, X.-Y. Dong, S.-Q. Zang and H. Hou, *J. Mater. Chem. A*, 2015, **3**, 12690–12697; (*c*) J. H. Qin, B. Ma, X. F. Liu, H. L. Lu, X. Y. Dong, S. Q. Zang and H. Hou, *Dalton Trans.*, 2015, **44**, 14594–14603; (*d*) J. H. Qin, H. R. Wang, Q. Pan, S. Q. Zang, H. Hou and Y. Fan, *Dalton Trans.*, 2015, **44**, 17639–17651; (*e*) J. H. Qin, H. R. Wang, M. L. Han, X. H. Chang and L. F. Ma, *Dalton Trans.*, 2017, **46**, 15434–15442; (*f*) J. H. Qin, Y. D. Huang and F. F. Li, *Inorg. Nano-Met. Chem.*, 2019, **49**, 7–11; (*g*) J. H. Qin, Y. D. Huang, Y. Zhao, X. G. Yang, F. F. Li, C. Wang and L. F. Ma, *Inorg. Chem.*, 2019, **58**, 15013–15016.

24 (*a*) J. Yang, L. Zhang, X. Wang, R. Wang, F. Dai and D. Sun, *RSC Adv.*, 2015, **5**, 62982–62988; (*b*) J.-C. Jin, J. Wu, Y.-X. He, B.-H. Li, J.-Q. Liu, R. Prasad, A. Kumar and S. R. Batten, *CrystEngComm*, 2017, **19**, 6464–6472.

25 (*a*) R.-X. Yao, X. Cui, X.-X. Jia, F.-Q. Zhang and X.-M. Zhang, *Inorg. Chem.*, 2016, **55**, 9270–9275; (*b*) L.-L. Gao, Q.-N. Zhao, M.-M. Li, L.-M. Fan, X.-Y. Niu, X.-Q. Wang and T.-P. Hu, *CrystEngComm*, 2017, **19**, 6651–6659.

26 (*a*) Y.-L. Gai, F.-L. Jiang, L. Chen, Y. Bu, K.-Z. Su, S. A. Al-Thabaiti and M.-C. Hong, *Inorg. Chem.*, 2013, **52**, 7658–7665; (*b*) J. Lu, C. Perez-Krap, F. Trousselet, Y. Yan, N. H. Alsmail, B. Karadeniz, N. M. Jacques, W. Lewis, A. J. Blake, F.-X. Coudert, R. Cao and M. Schroeder, *Cryst. Growth Des.*, 2018, **18**, 2555–2562.

27 O. V. Dolomanov, L. J. Bourhis, R. J. Gildea, J. A. K. Howard and H. Puschmann, *J. Appl. Crystallogr.*, 2009, **42**, 339–341.

28 G. Sheldrick, *Acta Crystallogr., Sect. A: Found. Adv.*, 2015, **71**, 3–8.

29 G. Sheldrick, *Acta Crystallogr., Sect. C: Struct. Chem.*, 2015, **71**, 3–8.

30 R. Q. Zou, R. Q. Zhong, M. Du, T. Kiyobayashi and Q. Xu, *Chem. Commun.*, 2007, 2467–2469.

31 (*a*) X. Liu, R. Li, L. Ma, X. Feng and Y. Ding, *New J. Chem.*, 2016, **40**, 619–625; (*b*) X. Yang and D. Yan, *Chem. Sci.*, 2016, **7**, 4519–4526; (*c*) A. Y. Ni, Y. Mu, J. Pan, S. D. Han, M. M. Shang and G. M. Wang, *Chem. Commun.*, 2018, **54**, 3712–3714; (*d*) Y. Zhao, X.-G. Yang, X.-M. Lu, C.-D. Yang, N.-N. Fan, Z.-T. Yang, L.-Y. Wang and L.-F. Ma, *Inorg. Chem.*, 2019, **58**, 6215–6221; (*e*) X. G. Yang, X. M. Lu, Z. M. Zhai, Y. Zhao, X. Y. Liu, L. F. Ma and S. Q. Zang, *Chem. Commun.*, 2019, **55**, 11099–11102; (*f*) X. G. Yang, Z. M. Zhai, X. M. Lu, Y. Zhao, X. H. Chang and L. F. Ma, *Dalton Trans.*, 2019, **48**, 10785–10789.

32 (*a*) S. M. Aly, M. R. Parida, E. Alarousu and O. F. Mohammed, *Chem. Commun.*, 2014, **50**, 10452–10455; (*b*) A. a. O. El-Ballouli, E. Alarousu, M. Bernardi, S. M. Aly, A. P. Lagrow, O. M. Bakr and O. F. Mohammed, *J. Am. Chem. Soc.*, 2014, **136**, 6952–6959.